

See discussions, stats, and author profiles for this publication at: <https://www.researchgate.net/publication/320742952>

# Experimental study on off-axis scattering of flat top partially coherent laser beams when propagating under water in the presence of moving scatterers

**Article** in *Waves in Random and Complex Media* · October 2017

DOI: 10.1080/17455030.2017.1393120

CITATION

1

READS

26

## 2 authors:



**Svetlana Avramov-Zamurovic**

United States Naval Academy

**58** PUBLICATIONS **278** CITATIONS

[SEE PROFILE](#)



**Charles Nelson**

United States Naval Academy

**40** PUBLICATIONS **110** CITATIONS

[SEE PROFILE](#)

## Some of the authors of this publication are also working on these related projects:



RF sensors in network to detect/locate IR radiation (laser strike) [View project](#)



Fiber optic temperature sensors for laser strike detection [View project](#)

# Experimental study on off-axis scattering of flat top partially coherent laser beams when propagating under water in the presence of moving scatterers

S. Avramov-Zamurovic<sup>1\*</sup>, C. Nelson<sup>2</sup>

<sup>1</sup> *Weapons and Systems Engineering Department, US Naval Academy, 105 Maryland Avenue, Annapolis, MD 21402, USA*

<sup>2</sup> *Electrical and Computer Engineering Department, US Naval Academy, 105 Maryland Avenue, Annapolis, MD 21402, USA*

e-mail: [avramov@usna.edu](mailto:avramov@usna.edu)

Off-axis underwater scattering of spatially partially coherent Multi-Gaussian Schell-Model (MGSM) beams are compared with fully coherent Gaussian beams in both a stationary setting and in the presence of mechanically agitated scatterers in underwater environments. The analysis is carried out by comparing the mean intensities of scattered light, the normalized variance, and the scintillation index in various scenarios. Results indicate that fully coherent beams have increased off-axis scattered light variations in the presence of moving scatterers as compared with a spatially partially coherent MGSM beam. Additionally, in a stationary environment the coherent beam has less overall variations as expected due to the nature of constructing partially coherent MGSM beams. Metrics of normalized variance, scintillation index, and overall average intensity are discussed in the context of potential beam localization, reduced scattering, and off-axis detection.

Key words: off-axis scattering, scintillation, laser beam, underwater, partially coherent, moving scatterers.

## 1. Introduction

The motivation for our work is the investigation of properties of off-axis laser beam detection in underwater environments. While scattering in random media is explored in great detail in [1, 2] and a number of references explore off-axis laser beam scattering under the auspices of detection of a laser threat to a platform in the maritime environment [3-5], we seek to extend the literature to include the underwater environment with the focus on exploration of the experimental scattering for spatially pseudo partially coherent beams (PPCB). PPCBs are of interest in underwater scattering due to their potential to provide a reduced off-axis detection signature. Our emphasis is the exploration of laser beam scattering in an approximately homogeneous medium and in a medium where scattering particles are mechanically agitated.

With regards to underwater propagation with entrained salts, Rayleigh scattering can be expected to play a role owing to the small size of scatter particles compared to the wavelength of laser propagation. Rayleigh scattering from spatially PPCBs with a flat top profile has been theoretically investigated [6] where it is suggested that scattering is reduced when coherence is decreased. Additionally, theory suggest that the scintillations decline as the beams becomes less coherent [7, 8].

With regards to partially coherent beams and scattering, Jansson et al [9] and Gori et al [10] explored the theoretical and experimental effects of forward scattered partially coherent beams and showed that the angular spread increased with a decrease in spatial coherence which could allow for types of laser beam discrimination.

Gbur and Vissar [11] provide an overview of the structure of partially coherent beams and list several achievements. In particular, Huttenen and al [12] state a strong impact of reduced scattering intensity of the field by scattering from microstructures in the case of reduced spatial coherence of the laser beam.

The experiments presented in this paper investigate the average intensity and the variations in the intensity of the scattered light from suspended particulates as compared to moving particles when spatially partially coherent laser beams propagate through water with entrained salts. To our knowledge no experiments exploring the intensity variations of off-axis scattered light effects of spatially partially coherent beams scattering from stationary medium and in the presence of moving particulates underwater environment have been carried out.

The paper is organized as follows. The experimental set up is presented in section 2. We introduce multi-Gaussian Schell Model beams that have flat top profile in section 3. In section 4 we describe the data processing methods used to analyze the results and in section 5 we present the findings of our research. Section 6 concludes this paper.

## **2. Experimental set up**

Our objective was to experimentally explore the scattering of spatially PPCBs in an underwater environment through both homogeneous regimes as well as those with moving scatterers in a laboratory environment. To this end, a stabilized HeNe laser source at 632.8 nm with a power of 2 mW and a beam expander were used to generate a Gaussian laser beam. A spatial light modulator (SLM) with a spatial resolution of 256 x 256 pixels, a sensor area of 6.14 mm x 6.14 mm was used to modulate the light. Eight thousand screens with prescribed statistics cycled at the rate of 333 Hz was used along with a beam expander to fill the SLM screen was used to generate the PPCBs.

The PPCB is an experimental realization of a partially coherent beam (PCB) where the beam is physically limited by how fast individual source realizations are produced as compared with the detection rate and atmospheric turnover time. References [13-15] discuss and explore PPCBs in theory, simulation, and experiment in greater detail.

A one-meter long water tank with a 10 cm x 10 cm of cross section was filled with distilled water. The laser beam was propagated through air for about 5 m before passing through the water tank. Sea salt was added to the water in order to provide entrained scatterers where water salinity was 41g/L with water temperature of 20.8 C. These conditions produce Rayleigh scattering due to the size of the salt molecules dissolved in the distilled water where a NaCl molecule size is on the order 0.2 nm.

Orthogonally to the laser beam propagation path, a camera was placed one meter away from the axis and used a 50 mm lens and a red notch filter. The field of view along the propagation path covered an approximately 10 cm length of laser beam scattering (see Figure 1). The camera had

a spatial resolution of 480 x 640 pixels and an intensity resolution of 14 bits. Additionally, for each data run, approximately 500 images were collected at a rate of 3 Hz and with an exposure time of 333 ms which was well under the 333 Hz cycling rate of the SLM allowed for a beam more closely represented by a theoretical partially coherent beam vs. pseudo partially coherent beam. Additionally, the approximate coherence time of the HeNe is on the order of a nanosecond which is much less than the detector response time and places the experiment in the regime of a “slow detector [16].”

The experiments were conducted in two medium regimes: a) still water with no (or minimal) motion of scattering particles and b) water mechanically perturbed by moving blades providing a low level motion of the scattering particles in the water. The still water regime with minimal particle motion was achieved by letting the water sit for approximately 24 hours before conducting the experiments. The steady state regime with low level of particle motion was achieved by exercising the mechanical blades for 15 minutes, then collecting measurements. A Gaussian beam (with no modulation by an SLM) and a MGSM beam with various degrees of coherence were propagated and measured in each of the medium regimes. Note, MGSM beams are spatially partially coherent beams with a flat intensity cross section and a diameter dependent on the prescribed degree of coherence. Figure 1 shows the experimental setup.

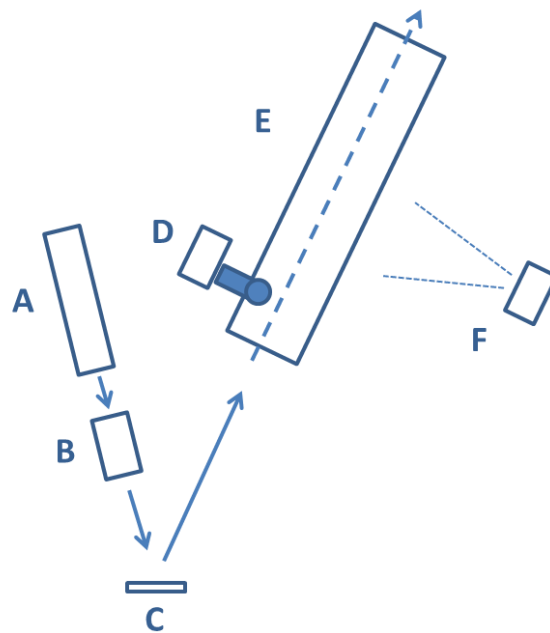


Figure 1. Experimental setup - A – HeNe laser, B – beam expander, C – spatial light modulator, D – mechanical agitator, E – 1 m propagation tank, F – camera.

### 3. MGSM beams

In this paper we will only give an overview of the theory behind the generation of the MGSM beams since there are a number of references [17-19] addressing the details of MGSM beam construction.

A recently developed model for the MGSM (flattop) beams, gives the following spectral (scalar) degree of coherence:

$$\mu^{(0)}(\rho_1, \rho_2) = \frac{1}{C_0} \sum_{m=1}^M \binom{M}{m} \frac{(-1)^{m-1}}{m} \exp\left[-\frac{|\rho_2 - \rho_1|^2}{2m\delta^2}\right], \quad (1)$$

where  $\rho_1$  and  $\rho_2$  are position distances and superscript (0) refers to the source plane,

$$C_0 = \sum_{m=1}^M \binom{M}{m} \frac{(-1)^{m-1}}{m}, \quad (2)$$

is the normalization factor used for obtaining the same maximum intensity level for any number of terms  $M$  in the summation, where  $\binom{M}{m}$  is the binomial coefficient. In Eq. (1),  $\delta$  is the r.m.s. width of the degree of coherence which describes the degree of coherence of the beam; where a value of  $\delta = 0$  gives a spatially incoherent beam and a value of  $\delta \rightarrow \infty$  gives a spatially coherent beam. Additionally, the upper index  $M$  relates to the flatness of the intensity profile formed in the far field:  $M = 1$  corresponds to the classical Gaussian Schell-Model source and  $M \rightarrow \infty$  corresponds to sources producing far fields with flat centres and abrupt decays at the edges.

Reference [20] provides general detail how one uses equations (1) and (2) to generate these spatially partially coherent beams by using an SLM. Additionally, the SLM phase screens were created in order to shift the first order ‘hot spot’ off of the beam propagation path utilizing a method developed by Hyde et al in [21-23] and further described for use with SLMs in [24].

#### 4. Data Processing Methods

The methodology used to analyse off-axis scattering of spatially PPCBs follow. We focus on characterizing the mean scattered light intensity and give a vector parameter in terms of averaged intensity across the image and single value parameter that gives total amount of scattered light in an image (section 4.1). To illustrate the light intensity fluctuations we present the normalized variance of the raw data and scintillation index derived from the image once the background was removed (section 4.2). Both parameters are vectors calculated across the image, orthogonal to the path of laser beam propagation path.

##### 4.1 Scattered light mean intensity

A Gaussian laser beam in the still water regime with minimal motion of scatterers is used in this section of the paper as the example to showcase the data processing steps. The Gaussian beam will be used as a relative benchmark to compare the measurements and trends with the spatially partially coherent beams. In addition, the results section of the paper will also demonstrate our findings using the spatially partially coherent MGSM laser beams.

The first step in our analysis is the representation of the mean scattered intensity,  $I_{avg}$ , from the beam propagating through the water. The image in Figure 2a) shows a matrix representation of the scattered light,  $I_{avg}$  from a Gaussian beam. Assuming that each image, ( $im$ ), is an  $m \times n$  matrix, with  $m = 480$  and  $n = 640$ , and that there are  $N = 500$ , images taken we find the matrix  $I_{avg}$  as:

$$I_{avg} = \frac{\sum_{j=1}^N (im)_j}{N} \quad (3)$$

The image of  $I_{avg}$  is a good qualitative observation to obtain insight into the scattered beam width and its mean peak intensity. Another representation of the data used is through the mean cross section calculated along the propagation path (represented summing along the dimension  $n$ ),  $I_{cross}$ , as:

$$I_{cross} = \frac{\sum_{j=1}^n I_{avg_{j,k}}}{n} \quad (4)$$

and the vector  $I_{cross}$  (with  $m$  elements) is shown in the Figure 2c). Since  $I_{avg}$  is a matrix, the  $m \times n$  are the matrix dimensions and the subscripts  $k$  and  $j$  are used to represent each element.

Figure 2b) is the three dimensional representation of Figure 2a) and shows in more detail the cross section view of the measured scattered light intensity along the propagation path averaged over the observation time. To obtain a performance characterization parameter,  $I_{cross}$  was obtained by averaging the scattered light measurements along the propagation path as shown in Figure 2c).

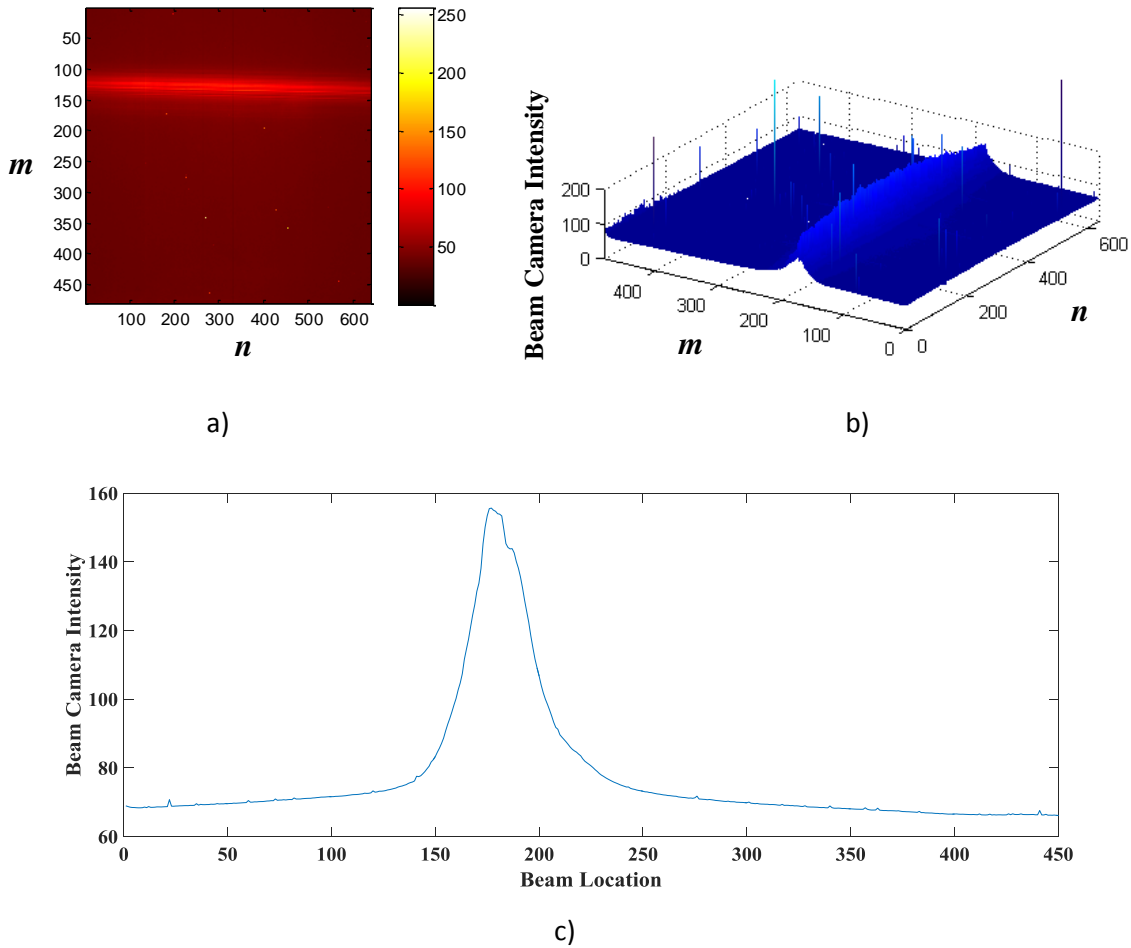


Figure 2. Measured scattered light from Gaussian beam propagating through water with low level motion of scatterers - a) Image of the average light intensity,  $I_{avg}$ , across the camera sensor

along the propagation path (camera view from Fig 1), b) 3 D plot of the image in a), c) Cross section average intensity,  $I_{cross}$  (this plot is the average along the path of the measurements as a function of pixel location shown in b). Note, in order to create a good qualitative illustration of the observed laser beam, the image in Figure 2 a) was constructed using a normalization to 256 intensity levels. This is in contrast to the cross-section plot in Figure 2 c) which shows the raw measured data averaged across the propagation path.

$I_{cross}$  demonstrates that most light is scattered from the centre of the beam (peak at value  $\sim 155$ ) and that there is a measurable glow (level at value  $\sim 68$ ) due to background noise as well as light scattered from the water volume. Notice that the measured scattering has a distinct shape that points to a) the sharp peak that locates the laser beam in space and b) the measurable width of the beam.

Additionally, to obtain an overall single value comparative parameter we calculate the mean value of  $I_{avg}$ ,  $MI_{avg}$ .  $MI_{avg}$  represents the total ‘raw’ averaged scattered intensity and gives an overall single value comparative parameter for the scattering  $MI_{avg}$ :

$$MI_{avg} = \frac{\sum_{k=1}^n \sum_{j=1}^m I_{avg,j,k}}{nm} \quad (5)$$

The parameters  $I_{cross}$  and  $MI_{avg}$  will be used to numerically compare the scattering from the laser beams in various conditions.

## 4.2 Scattered light variations

### 4.2.1 Variation method using raw data

A level of fluctuation of laser light scattered in the water can be expressed through the normalized variance,  $NV$ . The ratio of the variance of the fluctuating intensity of the laser light at a specified point in space over a course of the observation time, and the mean value squared, is in general defined as:

$$NV = \frac{Var(im)}{(Mean(im))^2} \quad (6)$$

In our case the  $(im)$  represents the images recorded experimentally and  $Mean(im) = I_{avg}$ . This result is a matrix and provides the normalized variance for the entire image calculated from raw data and is one of the parameters shown to be useful in locating the scattered laser beam position.

In order to observe the averaged  $NV$  along the propagation path, vector  $NV_{cross}$  is calculated similarly to eq. (4):

$$NV_{cross} = \frac{\sum_{j=1}^n NV_{j,k}}{n} \quad (7)$$

For a Gaussian beam (shown in the Figure 2), the normalized variance,  $NV$ , and the cross section of the normalized variance,  $NV_{cross}$ , are calculated using equations (6) and (7). Figure 3a) shows a very clear qualitative representation of the scattering along the propagation path of the beam. Figure 3b) shows the overlapped values of  $NV$  from Figure 3a) and is used as a representation

that demonstrates the  $NV$  peaks along the propagation path of the scattered light. Figure 3c) shows the  $NV$ , values from Figure 3 b) on one axis in order to highlight the range of some of the  $NV$  values seen along the propagation path. Figure 3 d) shows the  $NV_{cross}$  values. It is important to note that the  $NV_{cross}$  has the value of about 0.02 in the areas along the propagation path length where the beam is not propagating. This result agrees with the measured background noise,  $NV$  noise level (see Figure 4b)).

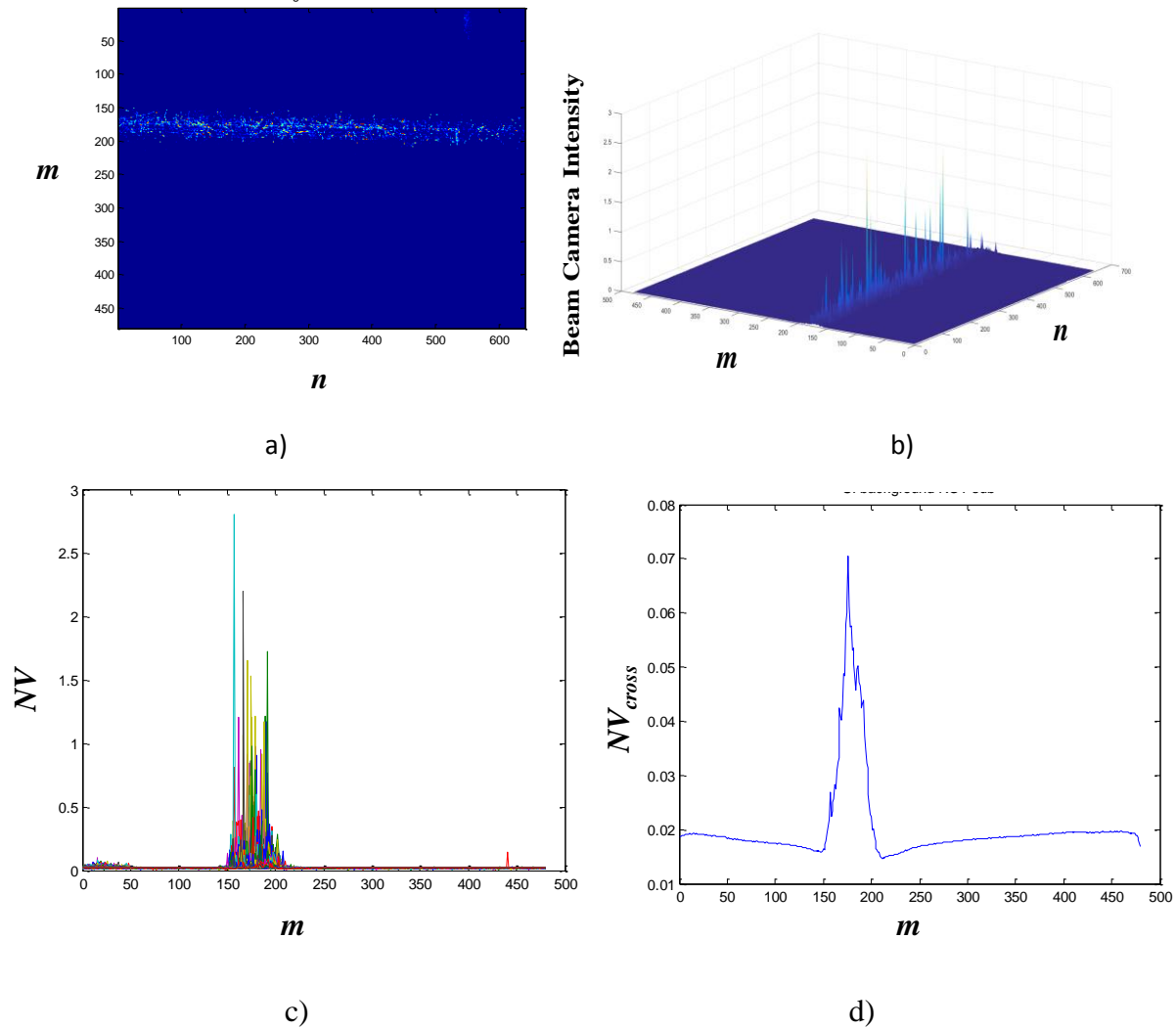


Figure 3. Calculated normalized variance from a Gaussian beam propagating through water with low level motion of the scatterers - a) The image of  $NV$  along the path of the laser propagation b) 3D look at the Fig. 3a values, c) Overlap of the peak variations along the path and d) Cross section normalized variance,  $NV_{cross}$ .

#### 4.2.2 Variation method with average background adjustment applied to each image (matrix approach)

The variance in the measured intensity is due to a) the laser light behaviour as it propagates and b) the camera electronic noise. To evaluate the effect of background noise, a set of images was recorded when the laser light was blocked. Figure 4 a) shows the  $I_{cross}$  of the measured average background intensity to be very consistent, at approximately 53.6 camera intensity, and Figure 4 b) shows the measured normalized variance,  $NV_{cross}$ , of the background to be approximately 0.0266 which is consistent with Fig. 3d and discussed in Sect. 4.2.1.

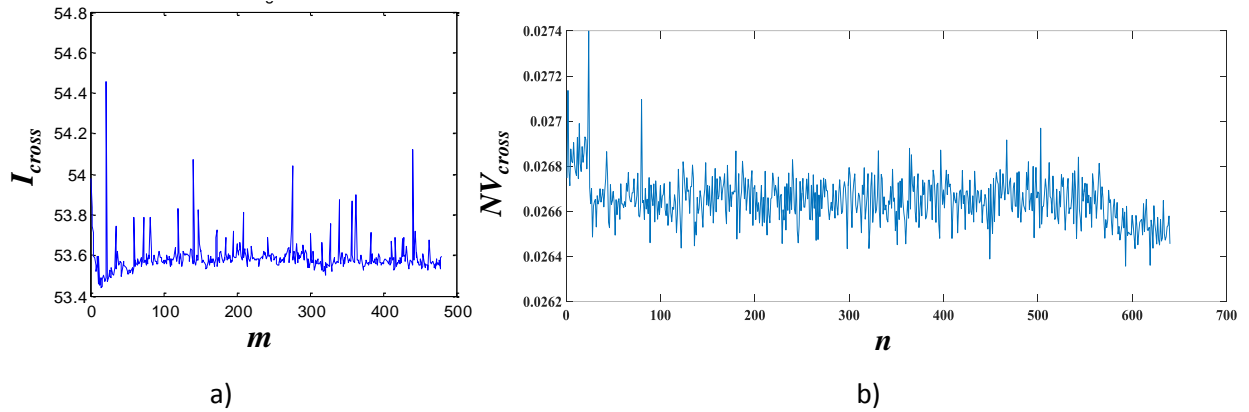


Figure 4. Measured camera background in the absence of laser light a) Cross section of the background average intensity,  $I_{cross}$ , b) Cross section of the background normalized variance  $NV_{cross}$ .

The spatial variance of the scattering along the laser propagation path with the background adjustment applied to each image is calculated as the scintillation index  $SI_B$ :

$$SI_B = \frac{\sum_{i=1}^N ((im_i - B_{avg}) - (I_{avg} - B_{avg}))^2}{N (I_{avg} - B_{avg})^2} \quad (8)$$

where  $B_{avg}$  is a single value parameter representing the average background intensity and calculated using eq. (5).  $SI_B$  is a matrix representing the scintillation index for each pixel in the image. We also introduce the cross section of the scintillation index,  $SI_{B\ cross}$ , a vector, calculated similarly as in eq. (4).

$$SI_{B\ cross} = \frac{\sum_{j=1}^n SI_{B\ j,k}}{n} \quad (9)$$

Figure 5 shows  $SI_B$  and  $SI_{B\ cross}$  for a Gaussian beam. Note, the  $SI_{B\ cross}$ , in the area where there is no laser light (see Figure 5b)) is relatively high compared to the measured variance of the noise (see Figure 4b)). In addition, the peaks in the laser propagation region (see Figure 5 and this was similarly seen in Fig. 4c)) are very high. The primary reason for this effect is the approximation of the background by using,  $B_{avg}$ , (its average value across the whole sensor area), instead of the instantaneous value for each pixel. This can be explained by the light intensity variations being intensified by subtracting mean background values which tend to mask

the intended measurements of the laser light scintillation in the low light level regimes. This effect is amplified with the faint laser light level and leads to inconclusive observations. Even though the normalized variance,  $NV$ , theoretically represents less scintillation, it is an effective practical tool to detect the laser light scattering trends in the complex media.

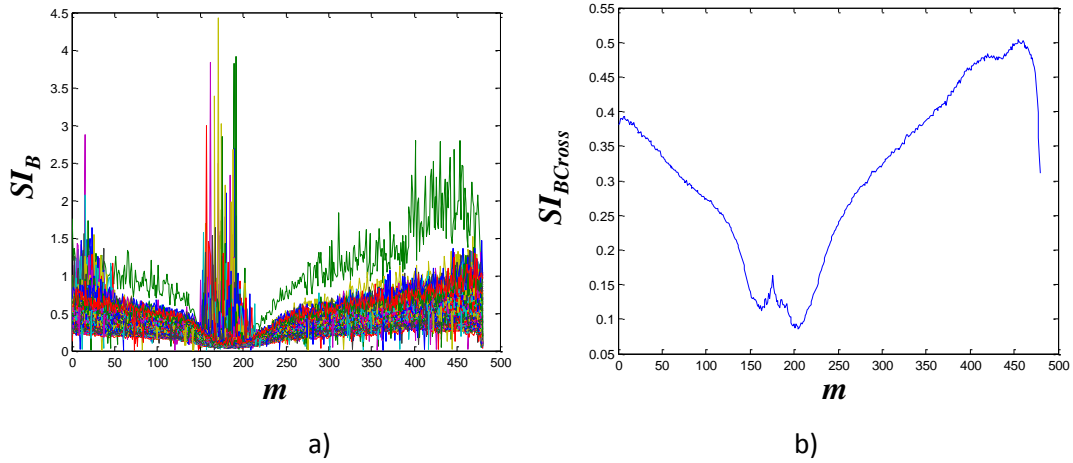


Figure 5. Calculated scintillation index  $SI_B$  from a Gaussian beam propagating through water with a low-level motion of scatterers,- a) Overlap of the peak variations of  $SI_B$  along the path. b) Cross section of the scintillation index,  $SI_{B\text{Cross}}$ . The x-axis gives the pixel number of the sensor cross section and the y-axis shows the scintillation index values.

#### 4.2.3 Variation method with average background adjustment applied to cross section average intensity (Vector approach)

There are 500 images taken for each measurement scenario,  $I_{\text{cross}}$ , was calculated for each image. The scintillation index was then obtained as the variance of the  $I_{\text{cross}}$ , over the observation time. This process minimizes the variations of the background noise in a frame, and also averages the laser light fluctuations along the laser path. The vector  $SI_c$  was computed as follows (Figure 6b):

$$SI_c = \frac{\frac{\sum_{i=1}^N ((I_{\text{cross}} - B_{\text{avg}}) - (I_{\text{avg}} - B_{\text{avg}}))^2}{N}}{(I_{\text{avg}} - B_{\text{avg}})^2}}{\quad} \quad (10)$$

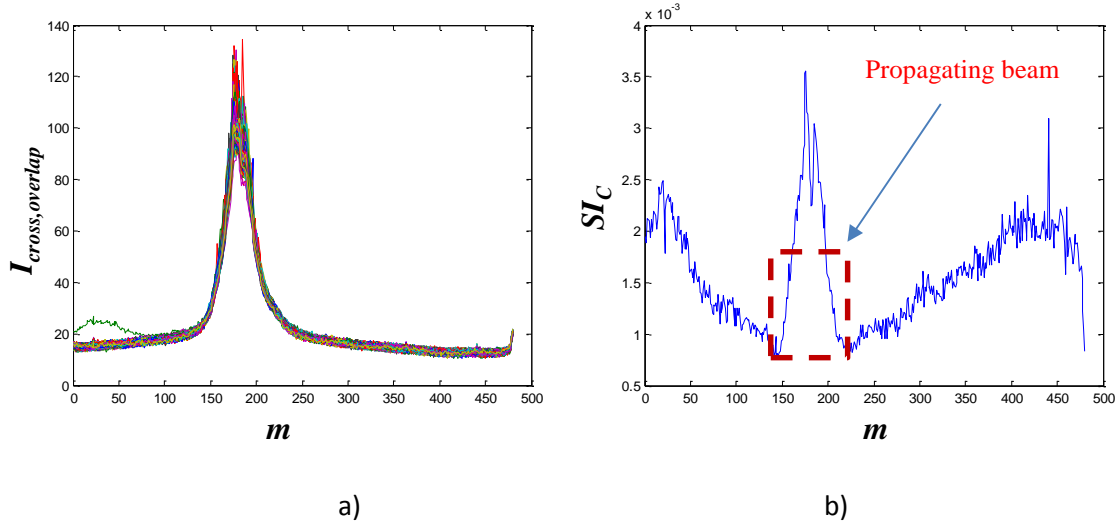


Figure 6. Gaussian beam propagating through water with low-level motion of the scatterers - a) Overlap of  $I_{cross}$  for each frame, b) Scintillation index  $SI_C$ . Note, the red box shows the location of the beam.

Figure 6a) shows the overlapped 500 individual  $I_{cross}$  realizations, with clear variations from frame to frame. The scintillation index for the  $I_{cross}$  was calculated using eq. (10) and  $SI_C$  is shown in Figure 6 b). Note that the scintillation is very low, partly due to the time averaging at a slow camera capture rate of 3 Hz as well as averaging along the laser path. In addition, there are higher levels of scintillation in the dim laser light area, but not as severe as in Figure 5. Note also that the scintillation pattern in the presence of laser light is very similar between Figures 3c), 5b) and 6b), with differences being in the value of the peak. This observation suggests that the observed trends will be similar among the presented methods of analysis.

## 5. Results

Gaussian beams (fully coherent), and PPCBs in the form of an MGSM where the degree of spatial coherence varied from less spatially coherent to more fully coherent, were compared. For the MGSM beam we chose to use a range of speckle sizes from 0.38 mm to 1.09 mm as measured at the SLM (method of calculation is described in [20]), where the larger speckle sizes indicate a more spatially coherent beam and the smaller size a more spatially incoherent beam. The goal was to compare the effects of varying the degree of spatial coherence on the scattered laser beam. Table 1 lists the experimental scenarios presented in the results section.

Table1. Experimental scenarios

Scenario	Beam type	Speckle radius [mm]	Scatterers motion
<b>A</b>	MGSM	0.38	Still water
<b>B</b>	MGSM	0.38	Low level
<b>C</b>	MGSM	1.09	Still water
<b>D</b>	MGSM	1.09	Low level
<b>E</b>	Gaussian	Coherent beam	Still water
<b>F</b>	Gaussian	Coherent beam	Low level

Note, spatially partially coherent beams (scenarios A-D in table 1) are created by modulating a Gaussian laser beam with a series of fast changing phase screens with prescribed statistics and this process introduces variations in the beam intensity by nature of the SLM cycling process. For this reason it may not be warranted to directly compare the performance of the Gaussian beam and MGSM beams. It is more sensible to compare the MGSM beams with different levels of coherence while maintaining the same cycling rate and as such, there can only be a qualitative trend comparison between the scatterings of Gaussian beam vs. the MGSM approximation of a coherent beam.

The results presented in the paper are taken from a set out of four identically run experiments. This representative set was chosen to demonstrate repeatable findings of our research.

### 5.1 Scattered light mean intensity

Figure 7 presents a summary of the scattered light mean intensity measurements for four different scenarios (A-D as described in Table 1). Notably, an MGSM beam with speckle radius of 0.38 mm (less spatially coherent) scatters the least when the laser is propagated through the still water (scenario A). The same beam propagated in the medium with low-level scatterer motion (scenario B) scatters more and the scattering pattern widens. An MGSM beam with the speckle radius of 1.09 mm (more spatially coherent beam), scatters the most with moving scatterers. Overall, for the more spatially coherent beam (scenarios C and D) the overall scattering is more intense including the peak, pattern width, and the side glow.

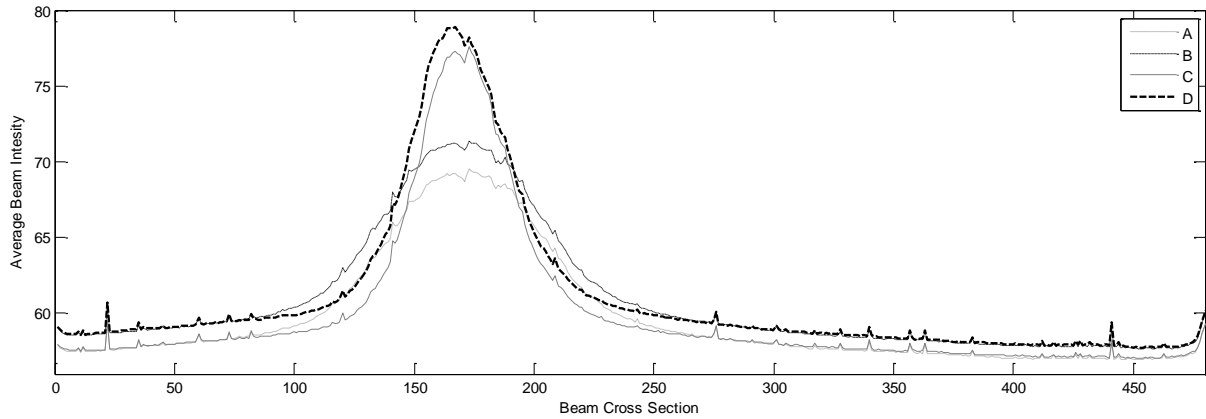


Figure 7. MGSM cross section average intensity,  $I_{cross\ avg}$  for four scenarios A- D. Note that the background level has not been adjusted.

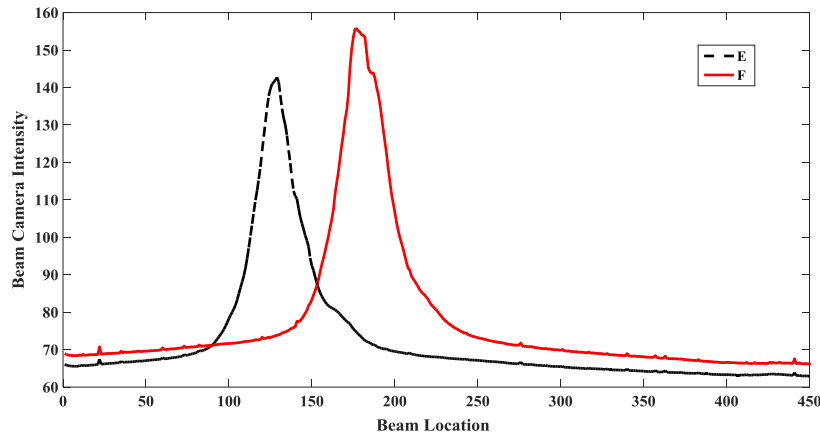


Figure 8. Gaussian cross section average intensity,  $I_{cross\ avg}$  for scenarios E and F. Note that the beams are at different locations due to the experimental adjustments. Note that the background level has not been adjusted.

Figure 8 shows a Gaussian beam propagating in two medium regimes: still water (scenario E) and with low-level scatterers motion (scenario F). It is clear that the motion of scatterers induces more scattering. It should be noted that the location of the beam moved from one experimental testing scenario to the next (as is evident with the beam shift in Figure 8), this was due to experimental sequencing and beam adjustment for optimal conditions. In addition, it is clear that relatively, the Gaussian beam scatters significantly more than the MGSM beams; but, this additional off-axis scattering was predominantly due to the influence of the additional beam power entering the water tank. In the case of Gaussian beam, 2 mW of laser power was propagated through the water, but in the case of the MGSM beams due to the method of their construction [18-20 ] only a fraction of 2 mW laser power actually enters the water tank. For this reason direct comparison between Gaussian and MGSM beams is not practical and thus the paper will focus only on trend comparisons.

Table 2 lists the values of the total scattered intensity  $MI_{avg}$  for the scenarios A-F with and without the background subtracted. Additionally, the scattered light intensity differences are summarized in Table 3a and 3b. Table 3a shows the trend of how the scattered light intensity of more coherent beam (speckle radius 1.09 mm) changes to the less coherent beam (speckle radius 0.38 mm). The more coherent beam scatters more in both regimes (values of 0.24 in both cases). Table 3b presents how each beam behaves when it goes from moving scatters to still water. The trends are more pronounced showing measured differences rising from 0.24 to 1.1 in both cases for the more coherent beam vs. less coherent beam. It is noteworthy to infer the trend that a Gaussian beam scatters significantly more than MGSM beams in the presence of moving scatterers as measured using the total average intensity value (value 4.5).

Table 2 Total scattered light intensity.

Scenario	A	B	C	D	E	F	Background noise $B_{avg}$
$MI_{avg}$	59.72	60.8	59.97	61.07	71.66	76.61	53.59
$MI_{avg} - B_{avg}$	6.14	7.24	6.38	7.48	18.07	23.02	

Table 3 Summary of the scattered light intensity trends.

a)

Measured differences in intensity	From scenario A to C Still water	From scenario B to D Moving scatterers
Change: speckle radius from 0.38 mm to 1.09 mm	0.24	0.24

b)

Measured differences in intensity	From scenario A to B Speckle size 0.38 mm	From scenario C to D Speckle size 1.09 mm	From scenario E to F Gaussian beam
Change: from still water to moving scatterers	1.1	1.1	4.5

## 5.2. Scattered light variations

The analysis of scattered light variations will include two methods: method of normalized variance as given in equations (6) and (7), and the method of scintillation index using an averaged cross section intensity as given in eq. (10). The two methods provide qualitatively complementary insights into how the light scatters.

The first column of Figure 9 shows the overlap of the peak  $NV$  values along the propagation path and the second column shows the  $NV_{cross}$  plot for scenarios A-D. Figure 9 represents the spatial distribution patterns of scattered light variations and the results are summarized in Tables 4 and 5a and 5b. The same comparison method is used as in Table 3a and 3b. Notably, the trend value going from scenario A to C (less coherent to more coherent in still water) decreases by 0.0024

which clearly shows that in still water there are less variations for a more coherent beam (speckle radius 1.09 mm) compared to the less coherent beam (speckle radius 0.38 mm). The trend is opposite (scenarios B to D), increasing by a value of 0.0085 which shows stronger variations in measured scattering when the beams propagate in the water with a low level of moving scatterers.

The peak  $NV$  values (the first column in Figure 9) provide a perspective into considerably more spatial variations in scattering of the MGSM beam with the radius of 1.09 mm vs. radius of 0.38 mm when the still water and the low-level scatterers' motion scenarios are compared.

This result suggests that a more coherent beam (speckle radius 1.09 mm) has noticeably higher variations of scattered light in the presence of moving scatterers. Note, the peak  $NV$  value in scenario D, Figure 9, is representative of the scattering cross section from a number of experimental tests in a low level scattering environment that we observed. This finding could prove useful in scattered laser beam detection algorithms. The plots of  $NV_{cross}$  (the second column in Figure 9) demonstrates averaged performance. The background noise is distinguishable as expected. Again, the most scattering is detected when coherent beam measurements are in the presence of moving scatterers.

Table 4. Summary of  $NV_{cross}$  measurements for scenarios A-D.

Scenario	A	B	C	D
<u>Selected (point on plot in Fig. 9) <math>NV_{cross}</math> values</u>	0.0186	0.0202	0.0162	0.0287

Table 5. Summary of normalized variance  $NV_{cross}$  trends.

a)

Measured differences in normalized variance	From scenario A to C Still water	From scenario B to D Moving scatterers
Change: speckle radius from 0.38 mm to 1.09 mm	-0.0024	0.0085

b)

Measured differences in intensity	From scenario A to B Speckle size 0.38 mm	From scenario C to D Speckle size 1.09 mm	From scenario E to F Gaussian beam
Change: from still water to moving scatterers	0.0016	0.0125	0.062

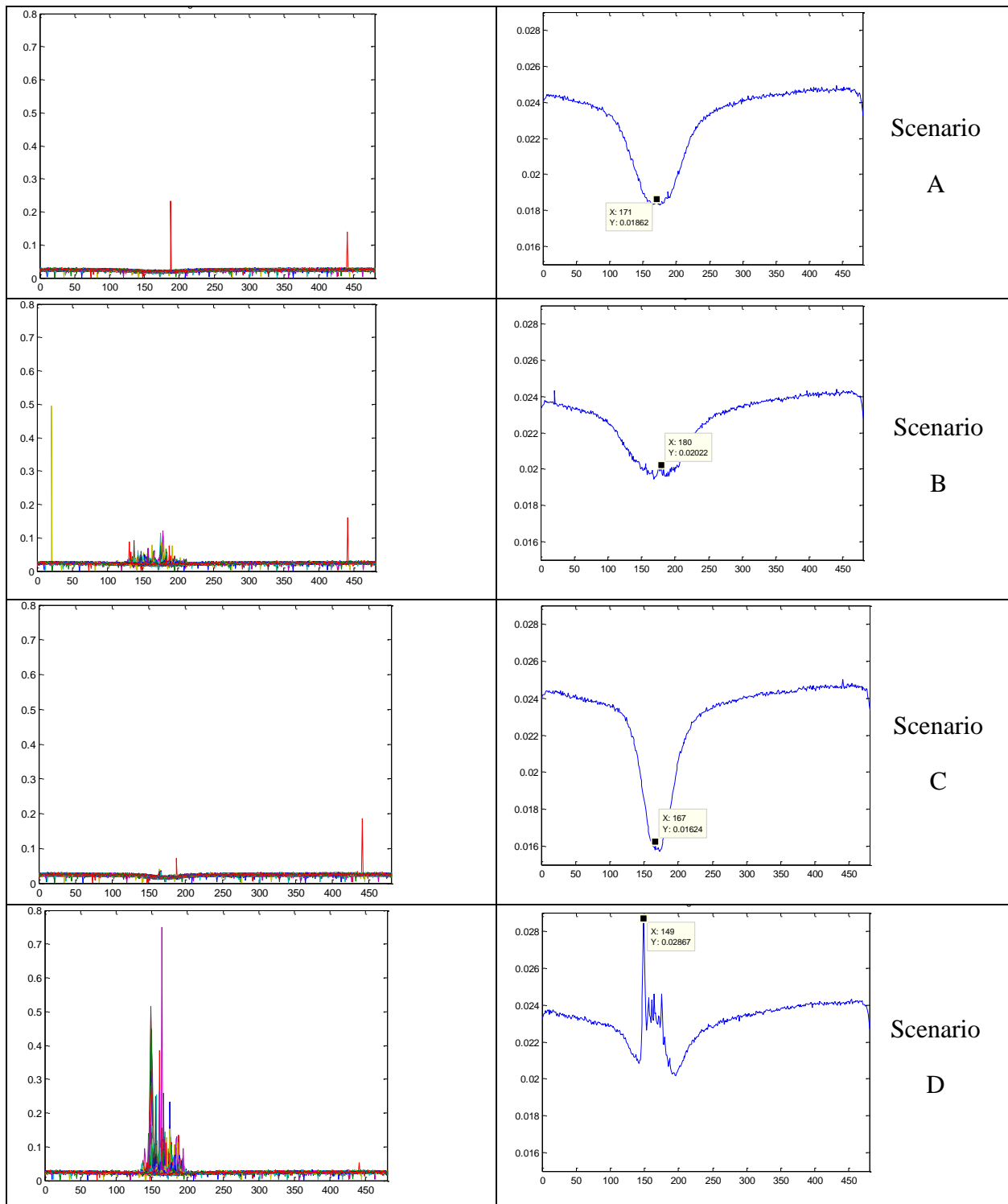


Figure 9. First column: Overlap of the peak variations of  $NV$  along the path. Second column: Cross section normalized variance,  $NV_{cross}$  for scenarios A-D. The x-axis gives the pixel number of the sensor cross section and the y-axis shows the normalized variance values.

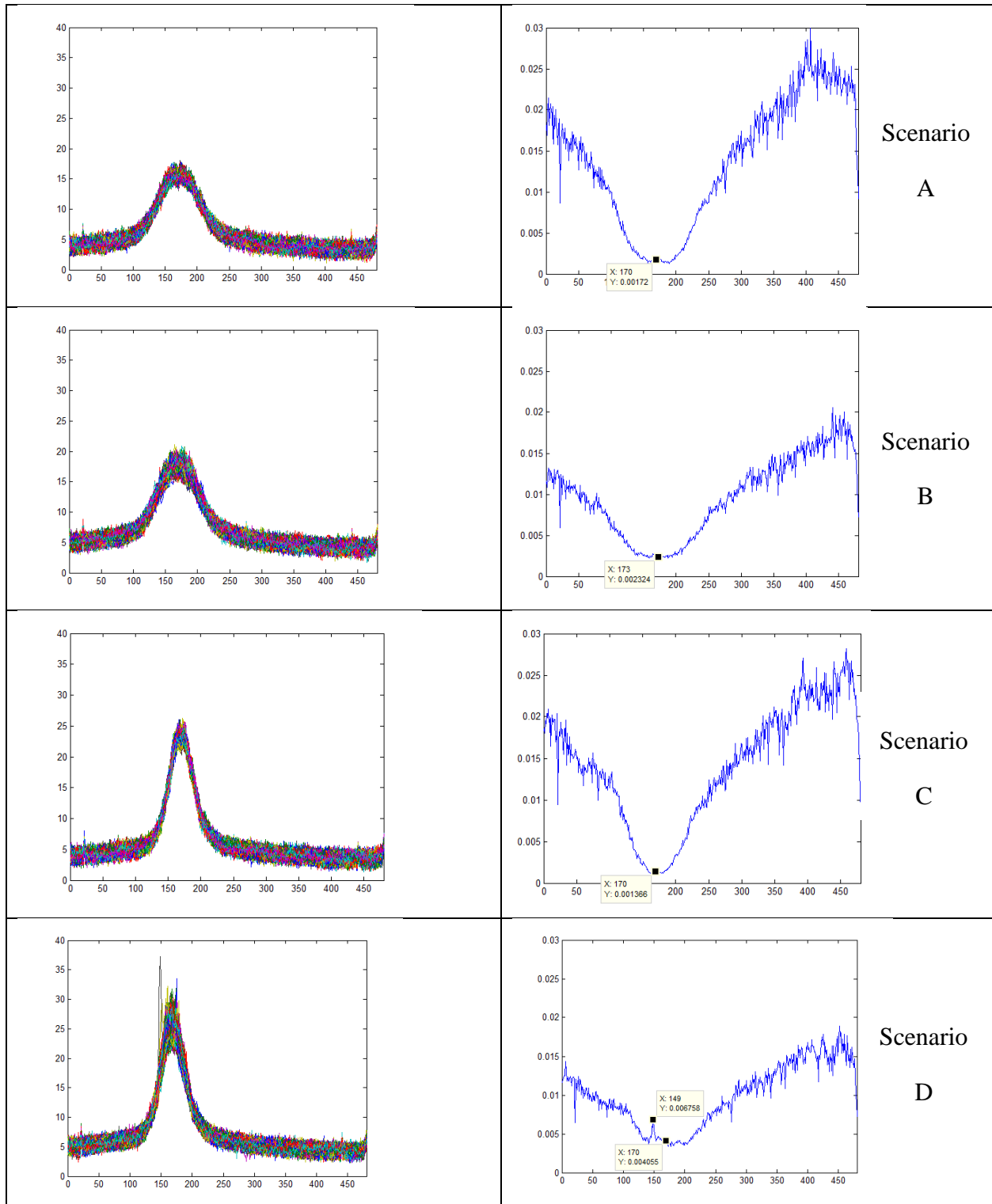


Figure 10. First column: Overlap of the  $I_{cross\ avg}$  along the path for each frame. The x-axis gives pixel number of the sensor cross section and the y-axis shows the camera intensity. Second column: Scintillation index using averaged cross section intensity,  $SI_C$  scenarios A-D. The x-axis gives pixel number of the sensor cross section and the y-axis shows the scintillation index values.

For the Gaussian beam, the increase of variations when we compared the beam propagating in the presence of moving scatterers to the still water propagation is the highest of all: 0.062. These outcomes suggest that scattered light varies substantially more in the presence of moving scatterers when beam is coherent.

Figure 10 shows the overlap of the  $I_{cross\ avg}$  along the path for each frame and the scintillation index,  $SI_c$  (Eq. 10) for scenarios A-D. The first column demonstrates the scattering variations and the spread for each frame. The scattering light reaches the peak value at the pixel 170, so this is the reference for the  $SI_c$  measurements in Table 6. Note that in scenario D there is a strong peak scintillation value at the pixel 149. This behaviour is a common occurrence in the presence of a larger moving particle from which the light scatters. The scintillation values are very low due to additional averaging (see eq. (10))

Table 6.  $SI_c$  measurements for scenarios A-D.

Scenario	A	B	C	D
$SI_c$	0.00172	0.002724	0.001366	0.00676

Table 7. Summary of scintillation  $SI_c$  trends.

a)			b)			
Measured differences in scintillation	From scenario A to C Still water	From scenario B to D Moving scatterers	Measured differences in intensity	From scenario A to B Speckle size 0.38 mm	From scenario C to D Speckle size 1.09 mm	From scenario E to F Gaussian beam
Change: speckle radius from 0.38 mm to 1.09 mm	-0.00354	0.004036	Change: from still water to moving scatterers	0.01	0.00539	0.0035

The observations in Figure 10 and Tables 6 and 7a and 7b demonstrate exactly the same trends as presented in Figure 9 and Tables 4 and 5. The difference is that in the former we have background noise adjusted and averaging across the propagation path was applied.

Figure 11 shows the Gaussian beam scintillation index  $SI_c$  in scenarios E and F. The scintillation index changes from 0.000059 (scenario E) to 0.003538 (scenario F) yielding the change of 0.00348. This result is in line with previous results.

These findings reinforce the notion that coherent beams appear to scatter more significantly in the presence of moving scatterers.

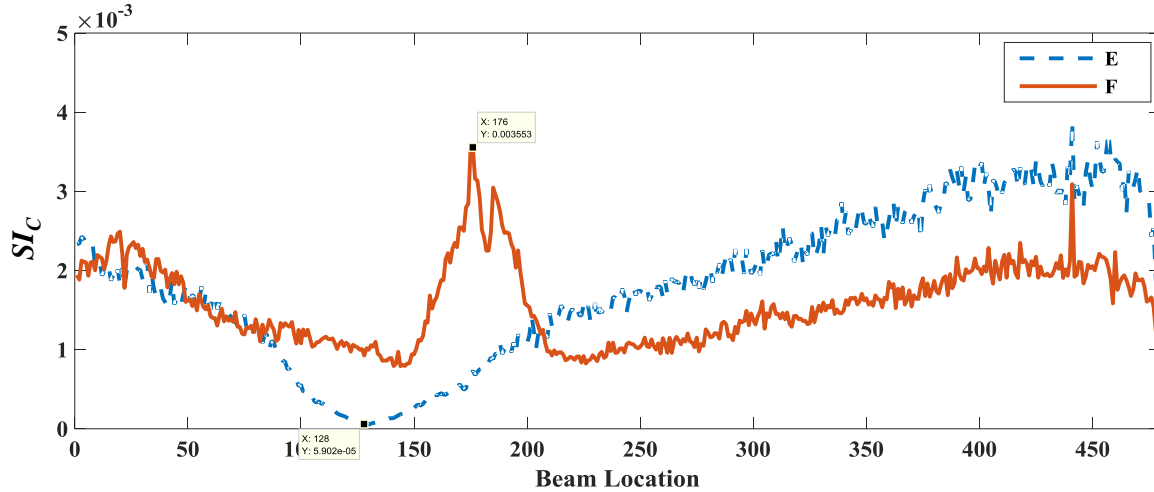


Figure 11. Gaussian beam scintillation index  $SI_c$  in the scenarios E and F.

## 6. Conclusions

We conducted a comprehensive experimental study of off-axis scattering of spatially PPCBs and coherent Gaussian beams in an underwater environment. The investigation demonstrated theoretical predictions that spatially partially coherent beams have less intensity variations when propagating and scattering in a complex medium, when compared with coherent beams. The research clearly shows the trend of influence of the laser light degree of coherence on underwater scattering and agrees with the overall understanding that due to a prescribed loss of spatial coherence (as in MGSM beams) the beamlets of laser light navigate the cluttered medium more effectively and thus scatter less. Our focus in this experiment has been the methodical observation of the scattered light underwater, leading to a future study of physical factors that drive its performance.

The measurements of scattered light scintillation suggest that spatially PPCBs could be used in scenarios requiring reduced scattering, as in detection algorithms that focus on search of laser light intensity fluctuations off-axis. Even though the results suggest that coherent beams fluctuations are less detectable in stationary environments, this may not prove to be a significant factor due to the realistic assumption that lasers propagate through complex media in all practical scenarios. Most importantly we observed that coherent light is significantly more influenced by changes in the environment compared to spatially PPCBs, leading to more volatile deterioration of the signal on the target. Additionally, mean intensity findings clearly show the possibility to localize the laser beams, with again, decreased scattering in the case of less coherent beams.

## 7. Acknowledgements

S. Avramov-Zamurovic is supported by US ONR grant: N0001414-WX-00267. C. Nelson is supported by US ONR grant N0001416WX00796.

## 8. References

- [1] A. Ishimaru, *Wave Propagation and Scattering in Random Media* (Academic, San Diego, Calif., 1978), Vols. 1 and 2.
- [2] M. Mishchenko, *Electromagnetic Scattering by Particles and Particle Groups*, (Cambridge University Press, 2014).
- [3] N. Roy, and F. Reid, "Off-axis laser detection model in coastal areas," *Optical Engineering* (2008).
- [4] F. Hanson, I. Bendall, C. Deckard, and H. Haidar, "Off-axis detection and characterization of laser beams in the maritime atmosphere," *Applied Optics*, (2011)
- [5] J. Kusmierczyk-Michulec, and R. Schleijsen, "Influence of aerosols on off-axis laser detection capabilities," *Proc. Of SPIE*, Vol. 7463 (2009)
- [6] Chengliang Zhao, Yangjian Cai, Xuanhui Lu, and Halil T. Eyyuboğlu, "Radiation force of coherent and partially coherent flat-topped beams on a Rayleigh particle", *Optics Express* Vol. 17, Issue 3, pp. 1753-1765 (2009)
- [7] Yahya Baykal, Halil T. Eyyuboğlu, and Yangjian Cai, "Scintillations of partially coherent multiple Gaussian beams in turbulence", *Applied Optics* Vol. 48, Issue 10, pp. 1943-1954 (2009)
- [8] Claudia Mujat and Aristide Dogariu, "Statistics of partially coherent beams: a numerical analysis", *JOSA A, Journal of the Optical Society of America A* Vol. 21, Issue 6, pp. 1000-1003 (2004)
- [9] J. Jansson, T. Jansson and E. Wolf, "Spatial coherence discrimination in scattering", *Optics Letters* Vol. 13, Issue 12, pp. 1060-1062 (1988)
- [10] F. Gori, C. Palma, and M. Santarsiero, "A Scattering Experiment with Partially Coherent Light," *Optics Communications*, (1990).
- [11] Gbur, G., and T. D. Visser. "The structure of partially coherent fields." *Progress in optics* 55 (2010): 285.
- [12] Juhani Huttunen, Ari T. Friberg, and Jari Turunen, "Scattering of partially coherent electromagnetic fields by microstructured media", *Phys. Rev. E* 52, 3081 – Published 1 September 1995
- [13] D. Voelz, and K. Fitzhenry, "Pseudo-partially coherent beam for free-space laser communication," *Proc. of SPIE* 5550, 218-224 (2004).
- [14] X. Qian, W. Zhu, and R. Rao, "Numerical investigation on propagation effects of pseudo-partially coherent Gaussian Schell-model beams in atmospheric turbulence," *Optics Express* Vol. 17, No. 5 (2009).
- [15] C. Nelson, S. Avaramov-Zamurovic, O. Korotkova, S. Guth, and R. Malek-Madani, "Scintillation reduction in pseudo Multi-Gaussian Schell Model Beams in the maritime environment," *Opt. Comms.* (2016)

- [16] L. C. Andrews and R. L. Phillips, *Laser Beam Propagation through Random Media*, 2nd ed. Bellingham, WA: SPIE Press, 2005
- [17] Korotkova, O., Sahin, S. and Shchepakina, E., "Multi-Gaussian Schell-model beams," *J. Opt. Soc. Am. A* 29, 2159- 2164 (2012).
- [18] Sahin, S. and Korotkova, O., "Light sources generating far fields with tunable flat profiles," *Opt. Lett.* 37, 2970-2972 (2012).
- [19] S Avramov-Zamurovic, C Nelson, S Guth, O Korotkova "Flatness parameter influence on scintillation reduction for multi-Gaussian Schell-model beams propagating in turbulent air", *Applied optics* 55 (13), 3442-3446, 2016.
- [20] Avramov-Zamurovic, S., Korotkova, O., Nelson C., and Malek-Madani, R., "The dependence of the intensity PDF of a random beam propagating in the maritime atmosphere on source coherence," *Waves in Complex and Random media* 24, 69-82 (2014).
- [21] M. W. Hyde IV, S. Basu, X. Xiao, and D. Voelz, "Producing any desired far-field mean irradiance pattern using a partially-coherent Schell-model source," *J. Opt.* 17 055607 (2015)
- [22] M. W. Hyde, S. Basu, X. Xiao, and D. G. Voelz "Producing any desired far-field mean irradiance pattern using a partially-coherent Schell-model source and phase-only control", *Imaging and Applied Optics 2015 OSA Technical Digest* (online) (Optical Society of America, 2015), paper PW3E.2.
- [23] M. W. Hyde, S. Basu, D. G. Voelz, and X.Xiao , "Experimentally generating any desired partially coherent Schell-model source using phase-only control ", *J. Appl. Phys.* 118, 093102 (2015);
- [24] S Avramov-Zamurovic, C Nelson, S Guth, O Korotkova, R Malek-Madani "Experimental study of electromagnetic Bessel-Gaussian Schell Model beams propagating in a turbulent channel ", *Optics Communications* 359, 207-215, 2016.